27.3 A 3-Axis Open-Loop Gyroscope with Demodulation Phase Error Correction

Chinwuba D. Ezekwe[1], Wolfram Geiger[2], Torsten Ohms[3]

[1]Robert Bosch, Palo Alto, CA,
[2]Robert Bosch, Reutlingen, Germany, [3]Bosch Sensortec, Reutlingen, Germany

Consumer-electronic (CE) gyroscopes have recently enjoyed broad deployment in high-volume applications, largely due to intuitive user interfaces in smart phones and video game controllers. For their continued expansion into more demanding CE applications, a further reduction of their noise, offset drift, and power dissipation, especially in the emerging *always-on* category, is mandatory. To be viable, solutions to these conflicting requirements must overcome the challenges of low cost and ever-shrinking package size. This paper describes one such solution with special emphasis on offset drift reduction. The system presented here discards the standard practice of electrically cancelling the quadrature error, and instead combines information derived from continuously monitoring the quadrature error together with a single-point temperature calibration to reduce offset drift. This paper presents the architecture and circuits used to realize a 3-axis open-loop gyroscope with a one-sigma TCO of 0.0065°/s/K.

Figure 27.3.1 illustrates a fundamental mechanism of offset drift in an open-loop vibratory gyroscope. A suspended mass is driven into a steady state oscillation in a drive axis. Under rotation, some of the *kinetic* energy in the drive oscillation couples onto a sense axis. Manufacturing imperfections also cause some of the drive oscillation to appear directly in the sense axis independent of rotation, a stress-sensitive coupling referred to as the quadrature error. Due to their modulation by the drive velocity and displacement respectively, the desired angular-rate and the unwanted quadrature-error signals are orthogonal, which, in principle, allows their discrimination via synchronous demodulation. However, the phase delay through the sense axis introduces a skew between the modulated signals and the demodulation clock, which allows a portion of the quadrature error to appear as an angular-rate signal at the output. For high yield, the magnitude of the acceptable worst-case quadrature error can exceed the full-scale angular rate by over 20dB, simultaneously placing a heavy burden on the dynamic range of the readout circuitry and very tight bounds on the phase error. To ease the dynamic range burden on the readout circuitry, state-of-the-art CE gyroscopes electrically cancel the quadrature error at the input of the sense channel capacitance-to-voltage (C/V) converter [1, 2]. However, besides the noise penalty that the cancelation signal injection incurs, the inevitable phase mismatch between the quadrature error and the cancellation signal can even exacerbate the offset drift problem.

The sensing element used in this work operates far below the sense resonance frequency, where the phase delay through the sense axis is inversely proportional to the quality factor of the sense resonance. While the quality factor varies with process and temperature, its temperature dependence when normalized to its value at a reference temperature is known and quite stable over process. This implies that the phase delay is $\phi \cong \phi(T_0)G(T_0,T)$, where T is temperature, T_0 is the reference temperature, and the function $G(T_0,T)$ is stable over process. Measurement at a single temperature point is, therefore, sufficient to predict the behavior of the phase delay over temperature. Fig. 27.3.2 illustrates how to exploit this opportunity to reduce the effect of the demodulation phase error. An I/Q demodulator separates the sense-axis oscillation into orthogonal components, which are respectively scaled by the weights $\sin\varphi$ and $\cos\varphi$ and recombined to advance the demodulation phase by $\varphi = -\phi$ and effectively undo the effect of the delay through the sense axis. Practically, the I and Q recombination weightings are simplified to unity and $-\phi$, respectively, with negligible penalty in accuracy since the phase error is typically on the order of 1°. Furthermore, the function $G(T_0,T)$, which is nonlinear in both T and T_0, is approximated as linear in T to further simplify the real-time computation. The dependence on T_0 is removed since the factory temperature remains within an acceptable range. The coefficients of G are estimated from the one-time measurement of a large number of samples.

Figure 27.3.3 shows the implementation of the concept, comprising a drive channel, three identical sense channels, a temperature sensor, and a digital backend. The drive channel consists of a C/V converter followed by a PLL and a drive amplitude regulator. Each sense channel consists of a C/V converter, a quadrature demodulator, and I and Q ADCs. The fully integrated PLL locks onto the drive displacement signal at the output of the drive C/V converter with negligible phase error and generates all timings, including the clocks used to perform the quadrature demodulation of the outputs of the sense C/V converters. These choices leave the delay through the sense axis as the dominant contributor in the signal chain. Demodulating in the analog domain enables the individual optimization of the I and Q ADCs for the power-and-area-efficient accommodation of the vastly different dynamic-and-input-range requirements of the I and Q sub channels. The ADCs are realized by single-bit $\Delta\Sigma$ modulators. Dynamic offset cancellation in the first integrators prevents the corruption of the down-converted signals by flicker noise. The temperature sensor comprises a PTAT reference followed by a $\Delta\Sigma$ modulator, whose first stage also employs dynamic offset cancellation. The seven $\Delta\Sigma$ bitstreams feed into the digital backend, where they are filtered and combined to produce the final low-drift output.

The circuitry described above implements the core function of the Bosch BMI160, a fully integrated 6-degree-of-freedom (6DOF) inertial measurement unit (IMU), requiring no external component beyond the usual V_{DD} bypass capacitors. The readout IC is implemented on a 1.8mm×2.7mm die in a 0.18µm standard CMOS process. The sensing elements are fabricated using Bosch surface-micromachining process with a 20µm poly-silicon structural layer and assembled with the readout IC in a 2.5mm×3.0mm×0.8mm plastic LGA package. With a supply voltage range of 1.71V to 3.6V, and an input range of ±2000°/s, the BMI160, during full gyroscope operation, draws less than 850µA, of which 650µA is spent on the complete mixed-signal core, including the regulators and references, and the remainder is spent on the digital backend and I/O interface. Fig. 27.3.4 shows the output noise spectra of a typical sample for an output data rate of 1.6kHz. With a flat power spectral density of 0.007°/s/√Hz in each axis from well below 1Hz to the maximum -3dB bandwidth of 520Hz, the BMI160 is suitable for noise-and-latency-sensitive applications, such as optical image stabilization and virtual reality as well as power-sensitive mobile applications. Fig. 27.3.5 shows the distribution of the temperature coefficient of offset (TCO) of 640 samples. The one-sigma TCO is 0.0065°/s/K in the worst axis. Fig. 27.3.6 compares the performance of this gyroscope to those of other state-of-the art gyroscopes [3-6]. These results validate the efficacy and economy of the approach presented here and set a clear new benchmark in CE gyroscope performance. Fig. 27.3.7 shows a micrograph of the readout IC.

Acknowledgement:
The authors thank the numerous colleagues across several Bosch business units who contributed to this development project.

References:
[1] J. Seeger, *et al.*, "Development of High-Performance, High-Volume Consumer MEMS Gyroscopes," *Solid-State Sensors, Actuators and Microsystems Workshop*, pp. 61-64. 2010.
[2] L. Prandi, *et al.*, "A Low-Power 3-Axis Digital-Output MEMS Gyroscope with Single Drive and Multiplexed Angular Rate Readout," *ISSCC Dig. Tech. Papers*, pp. 104-105, Feb. 2011.
[3] ST Microelectronics, "MEMS Motion Sensor: Three-Axis Digital Output Gyroscope," *L3GD20D datasheet*, 2013.
[4] Maxim Integrated Products, "Low-Power, Ultra-Accurate 6+3 DoF IMU," *MAX21100 Datasheet*, 2013.
[6] InvenSense, "MPU-6500 Product Specification," *MPU-6500 Datasheet*, 2014.

 978-1-4799-6224-2/15/$31.00

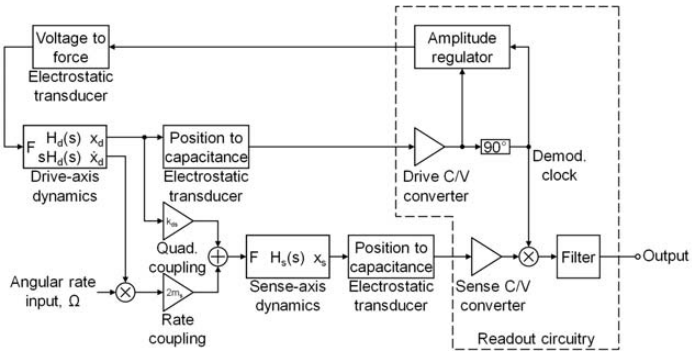

Figure 27.3.1: A fundamental mechanism of offset drift in an open-loop vibratory gyroscope.

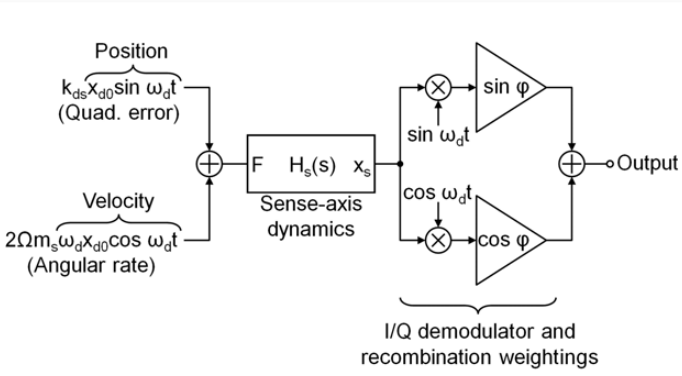

Figure 27.3.2: The concept of phase error correction illustrated with fixed angular-rate input and quadrature error.

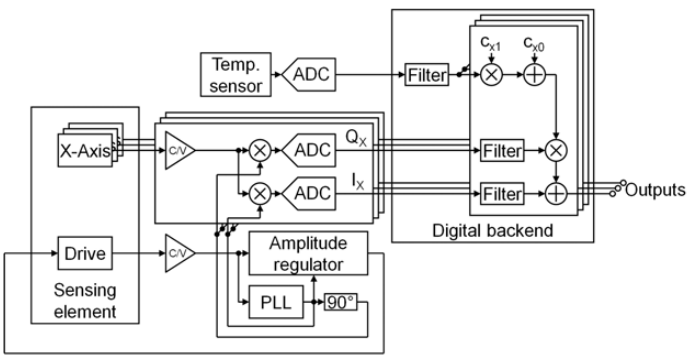

Figure 27.3.3: The implemented system.

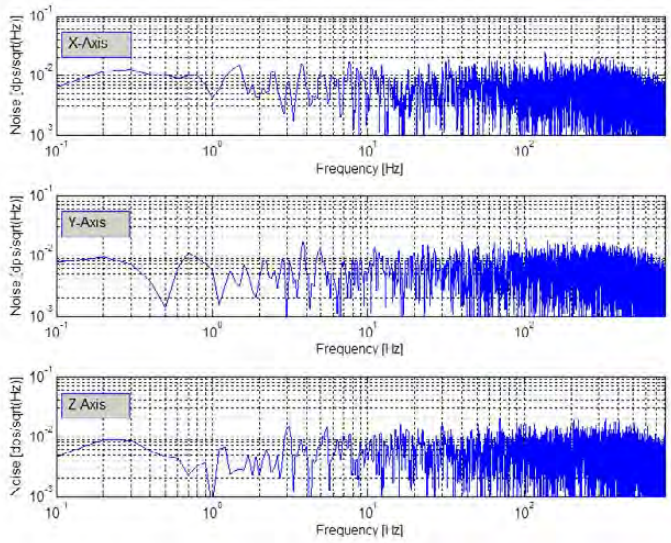

Figure 27.3.4: The measured output noise spectrum of a typical sample.

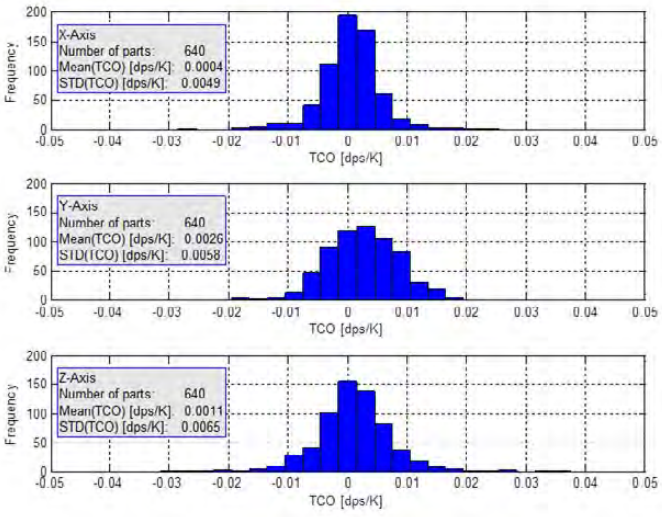

Figure 27.3.5: The distribution of the temperature coefficient of offset (TCO) of 640 samples.

Part	**This work BMI160**	InvenSense MPU-6500	ST Micro L3GD20	Maxim MAX21100
Package	**2.5x3.0mm²**	3.0x3.0mm²	4.0x4.0mm²	3.0x3.0mm²
Type	**6-DOF IMU**	6-DOF IMU	3-axis gyro	6-DOF IMU
V_{DD}	**1.71V - 3.6V**	1.71V - 3.6V	2.4V - 3.6V	1.71V - 3.6V
Input range	**±2000°/s**	±2000°/s	±2000°/s	±2000°/s
Supply current	**0.85mA**	3.2mA	6.1mA	5.4mA
Noise density	**0.007°/s/√Hz**	0.01°/s/√Hz	0.03°/s/√Hz	0.009°/s/√Hz
Max bandwidth	**520Hz**	250Hz	100Hz	2000Hz
TCO 1σ	**±0.0065°/s/K**	±0.24°/s/K	±0.04°/s/K	±0.025°/s/K
External components[1]	**none**	1 capacitor	1 capacitor	1 capacitor

[1]Excludes V_{DD} bypass capacitors.

Figure 27.3.6: Performance summary and comparison table.

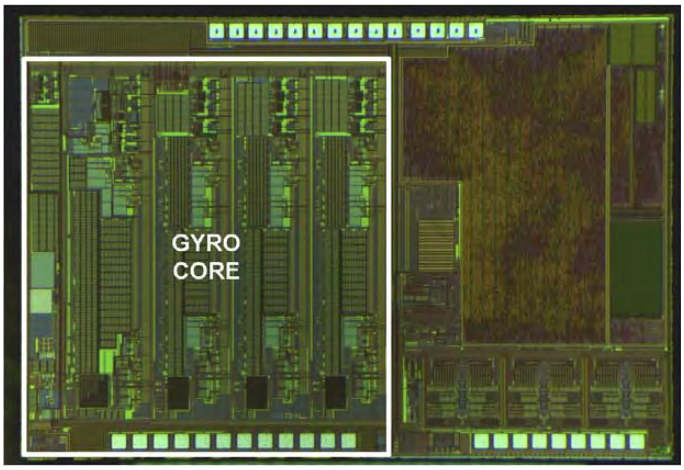

Figure 27.3.7: Die Photograph.

978-1-4799-6224-2/15/$31.00